

Full paper



## Reversible hybrid sodium-CO<sub>2</sub> batteries with low charging voltage and long-life

Changfan Xu<sup>a,b</sup>, Kaiwen Zhang<sup>a</sup>, Da Zhang<sup>a</sup>, Shilei Chang<sup>a</sup>, Feng Liang<sup>a,c,\*\*</sup>, Pengfei Yan<sup>d</sup>, Yaochun Yao<sup>a</sup>, Tao Qu<sup>a</sup>, Jing Zhan<sup>b</sup>, Wenhui Ma<sup>a</sup>, Bing Yang<sup>a</sup>, Yongnian Dai<sup>a</sup>, Xueliang Sun<sup>e,\*</sup>

<sup>a</sup> Faculty of Metallurgical and Energy Engineering, Kunming University of Science and Technology, Kunming, 650093, China

<sup>b</sup> School of Metallurgy and Environment, Central South University, Changsha, 410083, China

<sup>c</sup> State Key Laboratory of Complex Nonferrous Metal Resources Clean Utilization, Kunming University of Science and Technology, Kunming, 650093, China

<sup>d</sup> Beijing Key Laboratory of Microstructure and Properties of Solids, Institute of Microstructure and Properties of Advanced Materials, Beijing University of Technology, Beijing, 100124, China

<sup>e</sup> Department of Mechanical and Materials Engineering, University of Western Ontario, London, N6A 5B9, Ontario, Canada

### ARTICLE INFO

#### Keywords:

Na-CO<sub>2</sub> batteries  
N-doped single wall carbon nanohorns  
Aqueous catholyte  
Low polarization  
Good reversibility

### ABSTRACT

A reversible long-life hybrid Na-CO<sub>2</sub> battery is proposed by using Na<sub>3</sub>Zr<sub>2</sub>Si<sub>2</sub>PO<sub>12</sub> solid electrolyte as a separator, N-doped single-wall carbon nanohorns (N-SWCNH) as a catalyst and the saturated NaCl solution as an aqueous catholyte. The Na<sub>3</sub>Zr<sub>2</sub>Si<sub>2</sub>PO<sub>12</sub> ceramic not only has high Na<sup>+</sup> ion conductivity, but also prevents potential contamination from H<sub>2</sub>O and CO<sub>2</sub> to sodium anode, and avoids the internal short-circuit touch of Na dendrite with cathode, improving the safety of the battery. Benefiting from N dopants, unique internal and interstitial nanoporous structures, N-SWCNH have large surface area for discharge products accumulation, offer substantial structural defect sites for CO<sub>2</sub> adsorption and electron transfer, contributing to high catalytic activity and reversibility. Most importantly, the hybrid Na-CO<sub>2</sub> battery with aqueous electrolyte facilitates the dissolution of the insulated discharge product, which overwhelmingly improves the discharge and charge reactions kinetics. Na-CO<sub>2</sub> batteries exhibit a low charging voltage of 2.62 V and a small voltage gap of 0.49 V at a current density of 0.1 mA cm<sup>-2</sup>, a superior discharge capacity of 2293 mAh·g<sup>-1</sup> at a current density of 0.2 mA cm<sup>-2</sup>, a high round trip efficiency of ~68.7% after 300 cycles. In-situ Raman and ex-situ XRD analyses convincingly show that NaHCO<sub>3</sub> and carbon are the main discharge products.

### 1. Introduction

Excessive consumption of non-renewable fossil fuels such as coal, petroleum products, and natural gas has triggered worldwide concern for energy deficiency, furthermore, the corresponding carbon dioxide (CO<sub>2</sub>) emissions also has caused serious global warming and other increasingly deteriorative environmental issues [1,2]. Utilizing renewable energy sources such as solar energy, tidal, and wind power can alleviate the reliance on fossil fuels, but these renewable energies are unsteady and highly intermittent, as well as excessive storage cost [3,4]. Therefore, the development of advanced energy storage and conversion technologies is urgently needed in our daily life. Metal-CO<sub>2</sub> batteries, as a “killing two birds with one stone” strategy are figured to be an excellent candidate for next-generation energy conversion and storage

and CO<sub>2</sub> capture and utilization [5–8]. Exactly, the metal-CO<sub>2</sub> batteries can not only reduce fossil fuel consumption and mitigate the “greenhouse effect”, but also store intermittent renewable energy. Furthermore, owing to their high energy density, the future application of metal-CO<sub>2</sub> batteries will promote the development of the electric vehicle industry towards a more economical, environmentally friendly, and sustainable direction. In addition, metal-CO<sub>2</sub> batteries might also be of great significance for scientific exploration of space, for example 95% of gas on Mars is CO<sub>2</sub> [9].

The majority of research works have been carried out to study this new energy storage system since the initial Li-CO<sub>2</sub> batteries were successfully developed by Archer’s group in 2013 [5]. However, although scientists have focused on nonaqueous metal-CO<sub>2</sub> batteries for many years and significant breakthrough has been made, the development of

\* Corresponding author.

\*\* Corresponding author. Faculty of Metallurgical and Energy Engineering, Kunming University of Science and Technology, Kunming, 650093, China.

E-mail addresses: [liangfeng@kust.edu.cn](mailto:liangfeng@kust.edu.cn) (F. Liang), [xsun@eng.uwo.ca](mailto:xsun@eng.uwo.ca), [xsun9@uwo.ca](mailto:xsun9@uwo.ca) (X. Sun).

metal-CO<sub>2</sub> batteries are still relatively slow, which are impeded by poor recyclability, high polarization, and low rate capability due to the unstable electrolyte, sluggishness of electrochemical reactions at cathode [2]. High performance cathode can effectively promote the decomposition of discharge products and reduce the overpotential during charge and discharge, significantly improve the capacity and energy efficiency, as well as rate performance and cycle stability. Most of investigations have thus been explored toward catalysts such as Ketjen Black [7], super P [10], porous carbon [11], carbon nanotubes (CNT) [8,12–14], graphene [15], B, N-codoped holey graphene (BN-hG) [16], noble metal [17], metal-organic frame-works (MOFs) [18], as well as carbon supported metals and/or metal compound catalysts [19,20] for metal-CO<sub>2</sub> batteries. Unfortunately, all of above-mentioned catalysts seem to cause a high overpotential (>1.0 V) and poor recyclability in nonaqueous electrolytes, and the discharge products of carbonate are also extremely difficult to decompose unless at high voltages. Therefore, in addition to low catalytic activity cathode materials, the low electrochemical activity of CO<sub>2</sub> in nonaqueous electrolytes is also considered as one of the current major challenges [21].

Similar to metal-O<sub>2</sub> batteries, a suitable electrolyte is the key factor which affects energy density, cycling life, and safety for battery. Quasi-solid-state composite polymer electrolytes have been used in metal-CO<sub>2</sub> batteries to solve liquid electrolyte leakage, volatilization, and electrochemical instability [8,13,14]. Polymer electrolytes can alleviate infiltration of CO<sub>2</sub> and prevent the unnecessary side reactions between metal anode and CO<sub>2</sub>, but cannot effectively eliminate the influence of other impurity gases and water. In addition, the formation and growth of dendrites may penetrate the electrolyte separator, causing short circuits within the battery, triggering safety problems. Hence, further developing high chemical and thermal stability, high safety solid-state electrolyte for metal-CO<sub>2</sub> batteries to achieve high energy density and good stability is of great necessary. Na Super Ionic Conductor (NASICON) with superior structural stability, an effective structure to facilitate Na<sup>+</sup> diffusion has been widely studied as electrode materials [22], such as NASICON-structured Na<sub>2</sub>VTi(PO<sub>4</sub>)<sub>3</sub> served as not only as the cathode but also as the anode to construct a symmetric sodium ion batteries in aqueous electrolyte [23]. Recently, the concept of NASICON-type solid electrolyte Na<sub>3</sub>Zr<sub>2</sub>Si<sub>2</sub>PO<sub>12</sub> to protect sodium battery also have been successfully applied into rechargeable seawater batteries [24], redox flow battery [25], and hybrid sodium-air batteries [26–29]. Compared with other nonaqueous metal-air batteries, the batteries by using aqueous electrolytes could dissolve discharge products easily, thus successfully avoiding the blockage of porous gas electrode and ensuring the stable and sustainable operation of batteries [28,29].

Therefore, we propose an aqueous-nonaqueous hybrid Na-CO<sub>2</sub> battery using NASICON structured ceramic separator with the composition of Na<sub>3</sub>Zr<sub>2</sub>Si<sub>2</sub>PO<sub>12</sub> as solid electrolytes and N-SWCNH as the catalyst for the first time. The NASICON ceramic separator, as a solid electrolyte, is one of the key components in the hybrid Na-CO<sub>2</sub> batteries system with several advantages: (i) a 3D diffusion network allowing the transport of the single sodium-ion, which shows a high ion conduction exceeding 10<sup>-3</sup> S cm<sup>-1</sup> at room temperature [30], (ii) the metallic sodium and nonaqueous electrolyte are separated from the cathodic compartment, thus eliminating potential contamination from H<sub>2</sub>O and CO<sub>2</sub> to protect the sodium anode and nonaqueous, and (iii) avoiding the internal short-circuit touch of Na dendrite with cathode, improving the safety of the battery. Furthermore, the N-SWCNH with N dopants and unique nanoporous structures offer substantial structural defect sites for CO<sub>2</sub> adsorption and electron transfer. Most importantly, the aqueous electrolyte provides a potential route to solve the accumulation and blockage of insoluble discharge products, and increasing the limited contact area between discharge products and the catalysts, accelerating discharge products formation and decomposition. The as-prepared hybrid Na-CO<sub>2</sub> batteries not only demonstrated fantastic recycling performance and high capacities, but exhibited low charging voltage and voltage gap at a current density of 0.1 mA cm<sup>-2</sup>. This work indicates the

possibility of using aqueous-nonaqueous hybrid Na-CO<sub>2</sub> batteries to meet the demand of energy storage and fixing CO<sub>2</sub>.

## 2. Experimental

### 2.1. Preparation of catalytic cathode

The N-SWCNH was synthesized by direct current (DC) arc discharge method using nitrogen as buffer gas at a pressure of 70 kPa [31]. The catalytic cathode for hybrid Na-CO<sub>2</sub> batteries were composed of a gas diffusion layer (GDL), a catalyst layer, and a stainless steel mesh as the current collector. The GDL used in this work were fabricated by the following procedure [32]. Firstly, 15 mg of conductive carbon black (EBORY, China) and 10 mL of 5 wt% polytetrafluoroethylene (PTFE) emulsion were well mixed by sonication for 60 min, and then pre-knocked carbon paper (Toray, Japan) with diameter of 1 cm was immersed therein for 30 min. Next, the treated carbon paper was dried at 60 °C, which was then calcined at 450 °C for 60 min. The catalyst layer was prepared according to our previous work [33,34]. Four different catalyst slurries were prepared by dispersing 15 mg of N-SWCNH, single-walled carbon nanohorns (SWCNH, size = 30–100 nm XFNano Co. Ltd., Nanjing, China), gold nanoparticles (AuNPs, Aladdin), and N-doped MWCNTs (N-MWCNTs, XFNano Co. Ltd., Nanjing, China) in 2 mL of ethanol with a drop of 5 wt% PTFE as binder. The catalyst slurries were then homogeneously dropped onto the GDL, and the gas electrodes were obtained by pressing the catalyst layer onto the stainless steel mesh. In this work, the effective area of the Na-CO<sub>2</sub> battery was 0.79 cm<sup>2</sup> based on the battery model (Fig. S1), and catalyst loading was 2 mg cm<sup>-2</sup>.

### 2.2. Assembly of the hybrid Na-CO<sub>2</sub> battery

The electrolyte of 1 M NaClO<sub>4</sub> in EC/DMC (1:1) with 1 vol% FEC (Mojiesi Energy Company, China) was employed as nonaqueous anolyte. Solution of saturated NaCl was used as an aqueous catholyte. Around 0.2 mL of nonaqueous and aqueous electrolytes were used in the hybrid Na-CO<sub>2</sub> battery, respectively. A solid-state electrolyte Na<sub>3</sub>Zr<sub>2</sub>Si<sub>2</sub>PO<sub>12</sub> (NASICON) film was used as a separating membrane between the nonaqueous and aqueous electrolytes to prevent intermixing of these two solutions. The preparation of ceramic membrane of NASICON has been described in detail in our previous work [29]. The proposed hybrid Na-CO<sub>2</sub> batteries were assembled in a glove box filled with high purity argon (O<sub>2</sub> and H<sub>2</sub>O < 0.1 ppm) according to the following structure: metallic sodium | anolyte | NASICON | catholyte | catalytic cathode. For comparison, the batteries with nonaqueous electrolytes as catholyte were prepared by similar structure, only sodium chloride solution was replaced by 1 M NaClO<sub>4</sub> in EC/DMC (1:1) with 1 vol% FEC.

### 2.3. Electrochemical performance test

The assembled batteries were put into a glass container piped into the pure CO<sub>2</sub> (1 atm pressure). The charge and discharge tests were carried out on a LAND battery tester (CT2001A, Wuhan LAND electronics) at the temperature of 30 °C. The impedance measurements of the NASICON films were carried out using an electrochemical workstation (PARSTAT 4000 Rear Panel) in the frequency range of 0.1 Hz–10 MHz at room temperature.

### 2.4. Characterization techniques

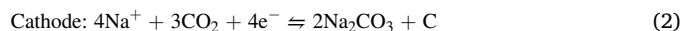
X-ray diffraction (XRD) patterns of the NASICON plate and the discharge products were measured using an X-ray diffractometer (MiniFlex 600, Japan) equipped with Cu K $\alpha$  radiation from 10° to 70° at a scan rate of 0.02°·s<sup>-1</sup>. The morphologies and microstructures characterizations of N-SWCNH were performed through scanning electron microscopy (SEM, SU8220, Hitachi) with acceleration voltage of 5.0 kV

and transmission electron microscopy (TEM, JEM-2100, JEOL) with acceleration voltage of 200 kV. The Brunauer-Emmett-Teller (BET) specific surface areas were calculated from the  $N_2$  adsorption isotherms. The Barrett-Joyner-Halenda (BJH) pore size distribution was analyzed with the adsorption branch data by using the non-local density functional theory (NLDFT) simulations. X-ray photoelectron spectroscopy (XPS) data were collected using a scanning XPS microprobe system (Kratos Axis Ultra DLD). Raman spectra of the N-SWCNH were obtained using a Renishaw Via Micro-Raman spectrometer (excitation wavelength, 514 nm). High-angle annular dark-field scanning transmission electron microscopy (HAADF-STEM) and energy-dispersive X-ray spectrometry (EDS) were conducted on a Titan G2 60–300 transmission electron microscope with probe corrector. The accelerating voltage is 300 kV. In situ Raman spectra were recorded on a laser confocal micro Raman spectrometer (DXRxi, Thermo Fisher) with an excitation wavelength of 532 nm using a homemade instrument with a quartz window for observation. Field-emission scanning electron microscopy (FE-SEM, MIRA3, TESCAN) equipped with an energy dispersive X-ray analyzer (EDX) and with acceleration voltage of 2.0 kV was used to examine the morphology and elemental composition of discharge products.

### 3. Results and discussion

Fig. 1a shows a typical structure of the hybrid Na-CO<sub>2</sub> battery, which is constructed as follows: Na | anolyte | NASICON | catholyte | catalytic cathode. Fig. 1b is the photo of practical hybrid Na-CO<sub>2</sub> battery. During the discharge process, the metallic Na was oxidized to Na<sup>+</sup> and transported into the cathode compartment after passing through the anolyte and NASICON, and the Na<sup>+</sup> combined with electrons and CO<sub>2</sub> to form Na<sub>2</sub>CO<sub>3</sub> and reduced carbon on the cathode. During charging, the

Na<sub>2</sub>CO<sub>3</sub> would combine with carbon to release Na<sup>+</sup>, electrons, and CO<sub>2</sub>, and then Na<sup>+</sup> could be migrated back and electrodeposited on the anode. The possible electrochemical reaction of cathode and anode for the hybrid Na-CO<sub>2</sub> battery are shown in equations (1) and (2) respectively, and the overall reaction follows as equation (3). The generated Na<sub>2</sub>CO<sub>3</sub> will combine with H<sub>2</sub>O and CO<sub>2</sub> to form NaHCO<sub>3</sub> in aqueous electrolyte during a long time discharge process as equation (4).



The ceramic solid electrolyte is the indispensable component for hybrid Na-CO<sub>2</sub> battery, which physically separates aqueous electrolyte and nonaqueous electrolyte, allowing Na-ion transfer between the anode and cathode [24]. The solid electrolyte affects coulombic efficiency, capacity, and recyclability of hybrid Na-CO<sub>2</sub> battery, a suitable electrolyte should satisfy the following requirements: (i) high sodium ionic conductivity and (ii) long-term stability against corrosion. Fig. 1c manifested the typical impedance profile of NASICON with a thickness of 1 mm and an effective area of 0.79 cm<sup>2</sup> as solid electrolyte at room temperature under ambient atmosphere. An equivalent electric circuit was applied to simulate EIS result, as shown in the inset of Fig. 1c [27]. The ionic conductivity of NASICON was measured to be  $1.6 \times 10^{-3} \text{ S cm}^{-1}$ , exhibiting highly sodium ion conducting behavior. The dense NASICON-typed Na<sub>3</sub>Zr<sub>2</sub>Si<sub>2</sub>PO<sub>12</sub> ceramic with a high specific density of 3.25 g cm<sup>-3</sup> is comparable to the theoretical density, the photo of practical Na<sub>3</sub>Zr<sub>2</sub>Si<sub>2</sub>PO<sub>12</sub> ceramic as shown in the inset of

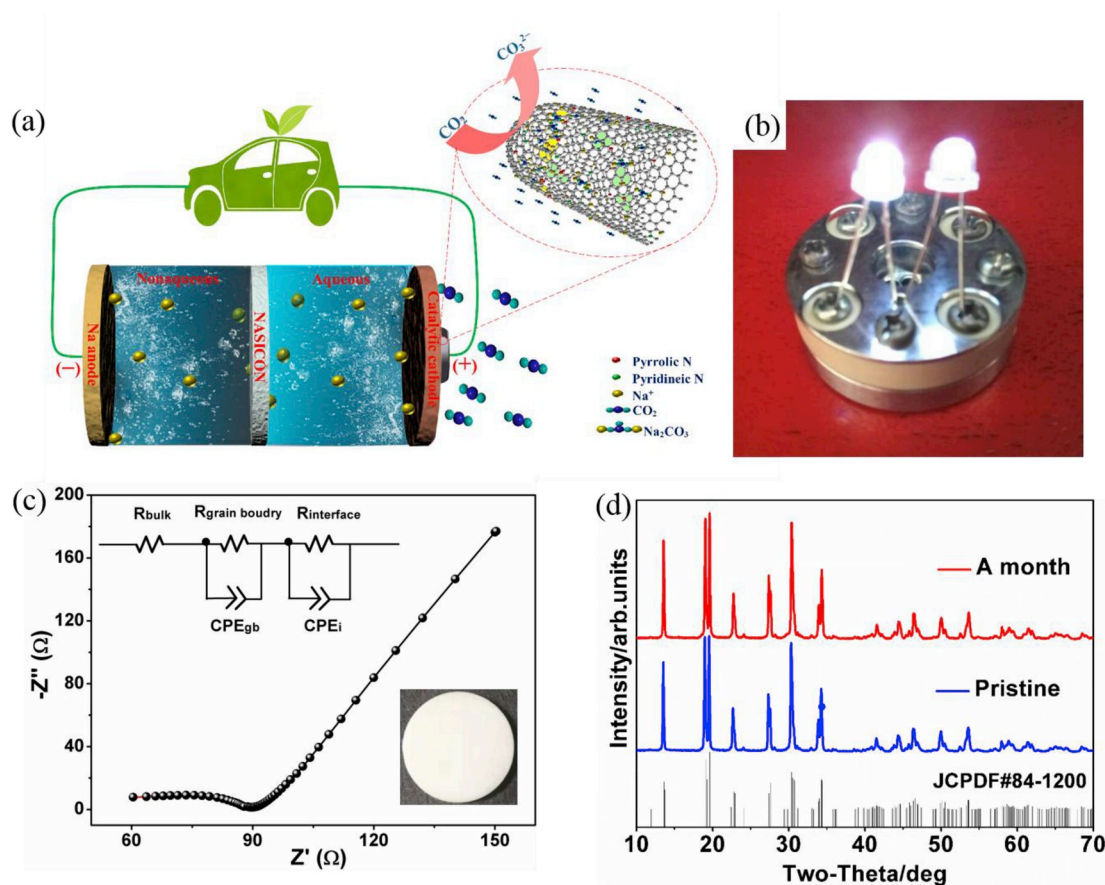


Fig. 1. (a) Schematic illustration of the proposed hybrid Na-CO<sub>2</sub> battery with N-SWCNH as a catalyst. (b) The photo of practical hybrid Na-CO<sub>2</sub> battery. (c) EIS analysis of NASICONs at 30 °C. (d) XRD patterns of NASICON as a function of immersion time in saturated NaCl aqueous solutions.

Fig. 1c. Additionally, the influence of the catholyte on the stability of the NASICON separator was investigated. As shown in Fig. 1d, the NASICON separator was immersed in the saturated NaCl solution at room temperature for 30 days with no significant change observed in the XRD pattern, indicating the NASICON separator is long-term stability in saturated NaCl solution. Hence, the NASICON separator was expected to be a potential candidate of solid electrolyte in a hybrid Na-CO<sub>2</sub> battery.

The typical scanning electron microscopy (SEM) and transmission electron microscopy (TEM) images of N-SWCNH are shown in Fig. S2 and Fig. 2a, respectively. As shown in Fig. S2, the N-SWCNH was clearly found to be consisted of uniform spherical aggregates with diameters of 30–80 nm on account of the van der Waals interaction [35]. As clearly seen in Fig. 2a TEM reveals the structure of N-SWCNH is the typical ‘dahlia-like’ aggregation ranging with size from 30 to 80 nm. The N-SWCNH typically is composed of a cone shape tip with cone angle of approximately 20° and a short cylindrical nanotube part [31,36]. From the HRTEM image (inset of Fig. 2a), the horn-shaped tips can be observed clearly. The cone shape termination with pentagons, hexagons and heptagons rings attributed to a well-ordered sp<sup>2</sup> carbon bonding structure on the tip [31]. A large number of pentagons and heptagons expose numerous potentially reactive sites in the structure. Fig. S3a showed the Raman spectrum of as-produced N-SWCNH, exhibiting the presence of two broad peaks, D and G bands, located at around 1350 cm<sup>-1</sup> and 1580 cm<sup>-1</sup>. The relative intensity ratio of the D band to G band (I<sub>D</sub>/I<sub>G</sub>) is 1.03, indicating that there are significant defect sites and a high disorder degree. Compared with I<sub>D</sub>/I<sub>G</sub> ratio of 0.94 for N-MWCNTs (Fig. S3b), the higher value I<sub>D</sub>/I<sub>G</sub> of N-SWCNH could be ascribed to pyramidal distortion of the sp<sup>2</sup>-bonded carbon and considerable carbon dangling bonds [36]. Moreover, HAADF-STEM was further employed to evidence the specific active sites of N-SWCNH. As shown in Fig. 2b, the nitrogen was homogeneously distributed amongst

carbon across the entire area, indicating the N elements were successfully doped in N-SWCNH. The high dispersion of N elements in the N-SWCNH as active sites would improve the electrocatalytic performance of N-SWCNH. The N-SWCNH also exhibited high porosity and huge specific surface area (Fig. S4), which is conducive to support substantial storage space for the discharge products. In order to further study the catalytic properties of the materials, XPS was used to characterize the chemical composition and the effects of nitrogen doping of N-SWCNH. As can be observed from C1s XPS data of N-SWCNH in Fig. 2c, the high-intensity peaks were correlated with the binding energy (284.8 eV) of sp<sup>2</sup> carbon atoms, and another two peaks located at 285.2 and 286.7 eV are attributed to the C=N and C-N bonds, indicating that nitrogen atoms have been successfully doped into the materials. The presence of structural nitrogen was further confirmed by N 1s peak in Fig. 2d. The doping level of N in the N-SWCNH catalyst was defined approximately 2.1 at.%, and the peaks positioned at 398.7, 399.6 and 401.4 eV were ascribed to the pyridinic N (14.79 at.%), pyrrolic N (45.96 at.%) and graphitic N (39.07 at.%), respectively [31,37]. The pyridinic N and pyrrolic N are beneficial to the electronic affinity, wettability and capacitance of N-SWCNH, and graphite N can improve the electronic conductivity and corrosion resistance of N-SWCNH [38]. Therefore, the unique structure of N-SWCNH has the potential to improve the electrocatalytic activities of Na-CO<sub>2</sub> batteries.

Electrochemical performance of Na-CO<sub>2</sub> batteries with different catholytes and using N-SWCNH as the catalyst at pure CO<sub>2</sub> conditions were investigated. As shown in Fig. 3a, the battery with nonaqueous electrolytes (1 M NaClO<sub>4</sub> in EC/DMC (1:1)) exhibited a low discharge voltage of 1.56 V and high charge voltage of 4.0 V, indicating the low electrochemical activity of CO<sub>2</sub> in nonaqueous electrolytes. In addition, the insolubility of the discharge product in nonaqueous electrolytes and high interfacial resistance between the NASICON and nonaqueous

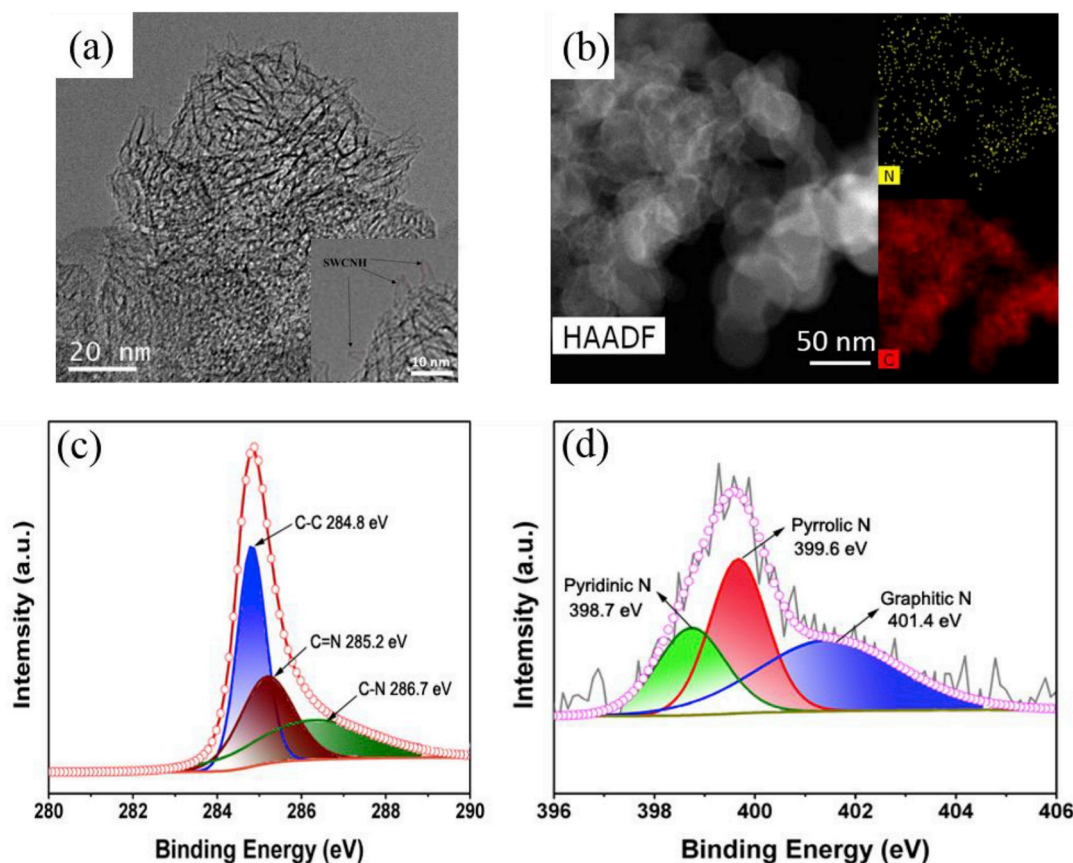
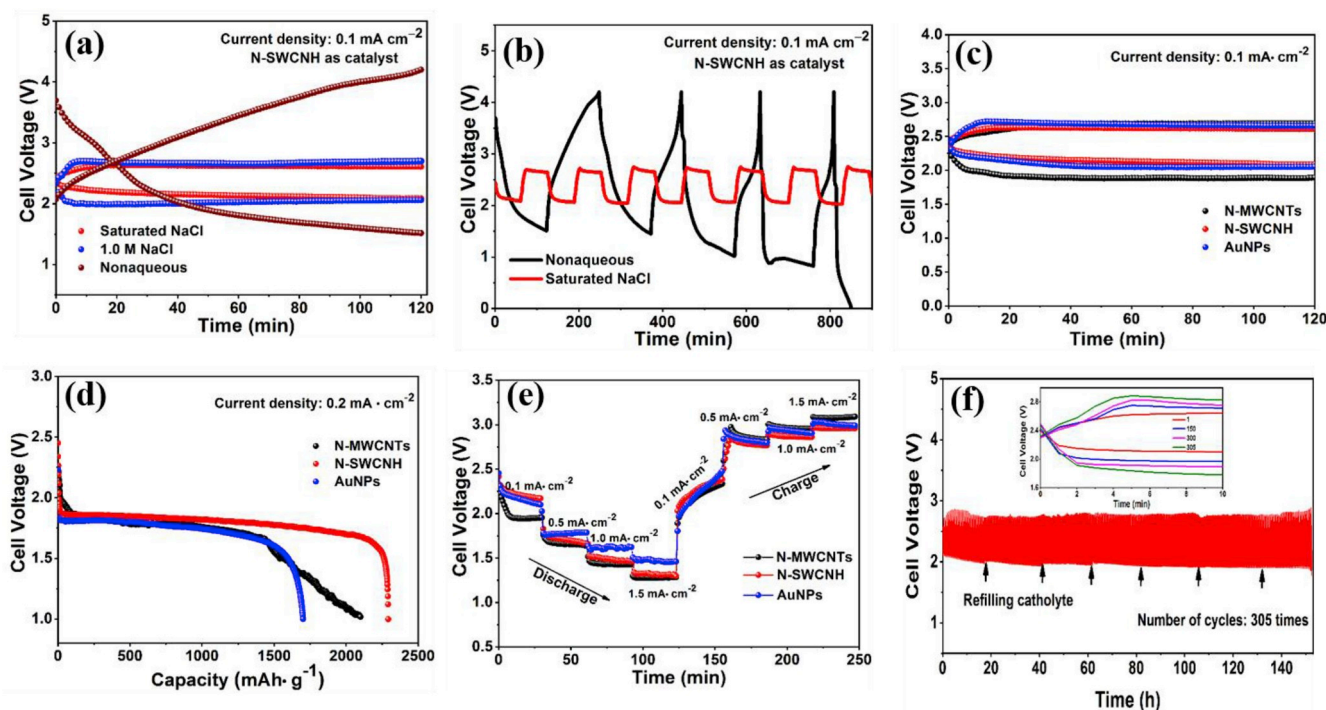


Fig. 2. (a) TEM and HRTEM (inset of Fig. 2a) image, (b) HAADF-STEM image of N-SWCNH and the corresponding elemental mappings of C and N (insets), (c) C1s and (d) N1s X-ray photoelectron spectra of N-SWCNH.



**Fig. 3.** Electrochemical performances of proposed Na-CO<sub>2</sub> batteries: (a) discharge-charge voltage curves with different catholytes at a current density of 0.1 mA cm<sup>-2</sup>, (b) cycling performance with different catholytes at a current density of 0.1 mA cm<sup>-2</sup>, (c) discharge-charge voltage curves with N-MWCNTs, AuNPs, and N-SWCNH as catalyst at a current density of 0.1 mA cm<sup>-2</sup>, (d) discharge capacities curves at a current density of 0.2 mA cm<sup>-2</sup>, (e) discharge and charge voltage profiles at different current densities, (f) the cycling performance of hybrid Na-CO<sub>2</sub> battery with N-SWCNH as catalyst at a current density of 0.1 mA cm<sup>-2</sup>.

electrolytes result in the sluggishness of discharge and charge reactions kinetics at cathode, the battery with nonaqueous electrolytes thus displayed poor discharge and charge behaviors. The effects of different concentrations aqueous electrolytes (1 M NaCl and saturated NaCl) on the battery also were studied (Fig. 3a). The battery with saturated NaCl electrolytes showed a low charging voltage and voltage gap than the battery with 1 M NaCl electrolytes, which could be attributed to the high Na<sup>+</sup> concentration and high ionic conductivity. As can be obviously seen from Fig. 3b, the battery with nonaqueous electrolytes exhibited terrible cycle performance, compared with conventional Na-CO<sub>2</sub> system, there are no obvious oxidation and deoxidation platforms in our hybrid Na-CO<sub>2</sub> batteries using NASICON-type solid electrolyte (Na<sub>3</sub>Zr<sub>2</sub>Si<sub>2</sub>PO<sub>12</sub>) as a separator and nonaqueous electrolyte as catholyte for the following reasons. Firstly, relatively high interfacial resistance of the current nonaqueous Na-CO<sub>2</sub> based on NASICON solid electrolyte separator is likely a critical cause for the slow kinetic reaction, which is caused by relatively low ionic conductivity of NASICON compared with the liquid-based counterpart at room temperature, and the high interfacial resistance between the NASICON and nonaqueous electrolytes. Moreover, mismatch between nonaqueous electrolyte and cathode also leads to the sluggishness of discharge and charge behavior. However, no distinct change of the charge and discharge voltage plateaus is observed from the battery with saturated NaCl electrolytes, indicating excellent charge/discharge cycle stability of the hybrid Na-CO<sub>2</sub> battery based on the saturated NaCl electrolytes. To be specific, sodium chloride aqueous solution for electrochemical storage have the advantages of abundant raw material, low cost, and mild reaction conditions, which would be great application prospects for future large-scale energy storage systems. A saturated NaCl solution as catholyte can effectively ensure the stability of the battery and improve the conductivity of the cathode electrolyte.

Fig. 3c shows discharge-charge voltage curves of the proposed hybrid Na-CO<sub>2</sub> batteries containing N-MWCNTs, AuNPs, and N-SWCNH as catalysts at a current density of 0.1 mA cm<sup>-2</sup> by controlling the

discharge/charge time of 2 h. The MWCNTs possess 3D tri-continuous porous structure, high electro-conductivity, and good wettability to nonaqueous electrolyte, which have been used by Chen et al. to fabricate Na-CO<sub>2</sub> batteries [8,14]. However, the hybrid Na-CO<sub>2</sub> battery with N-MWCNTs exhibited the lowest discharge voltage of 1.89 V compared to others, which is mainly determined by limited specific surface area, inferior wettability to aqueous electrolyte, and a small number of activation sites [39]. Generally, AuNPs were targeted as a great potential catalyst for CO<sub>2</sub> reduction reaction because it is reported to exhibit high activity and selectivity among polycrystalline metals [40,41]. A high discharge terminal voltage of 2.05 V was obtained for the AuNPs catalyst of hybrid Na-CO<sub>2</sub> battery. In addition, the battery containing AuNPs catalyst exhibited the desirable charge voltage of 2.66 V, which corresponded to the voltage gap of 0.61 V. Among them, the hybrid Na-CO<sub>2</sub> battery with N-SWCNH displayed the highest discharge voltage 2.13 V, while charging voltage of 2.62 V was slightly higher than SWCNH catalyst (2.61 V), which contributed to the high roundtrip efficiency of 81.3%. Excitingly, the hybrid Na-CO<sub>2</sub> batteries using the N-SWCNH catalyst demonstrated the most narrow voltage gap of 0.49 V compared to that of other Na-CO<sub>2</sub> batteries at a current density of 0.1 mA cm<sup>-2</sup> (Table S1). Noted that the hybrid Na-CO<sub>2</sub> battery with SWCNH exhibited a relatively low discharge terminal voltage of 1.95 V compared to the battery with N-SWCNH, indicating N-doping SWCNH was beneficial for enhancing the electrocatalytic performance of the catalyst for CO<sub>2</sub> reduction (Fig. S5). The metal-free N-SWCNH exhibited excellent electrocatalytic behavior for CO<sub>2</sub> reduction, which can mainly be ascribed to their unique conical structure and effective nitrogen doping. The unique porous structure and large specific surface area can facilitate the electrolyte/CO<sub>2</sub> diffusion and electron transport. Moreover, unique conical structure has more space for discharged products to deposit in, thus the battery with N-SWCNH showed the low charge voltage. Not only that, substantial pentagons and heptagons provide potentially defect sites for N-SWCNH, which enables the possibility to optimize the wettability, the electronic affinity, and the capacity adsorption/desorption of CO<sub>2</sub> [42].

In addition, the N dopants also increased numerous catalytic sites, thus enhancing the CO<sub>2</sub> reduction kinetics, and improving the electrochemical activity of hybrid Na-CO<sub>2</sub> battery [16,43].

In this work, all achieved specific capacity values were characterized to the weights of catalysts. The discharge capacities of the batteries were calculated at a fixed current density of 0.2 mA cm<sup>-2</sup> and cut-off voltage of 1.0 V. As we can see from the voltage-capacity profiles of hybrid Na-CO<sub>2</sub> batteries in Fig. 3d, high discharge capacity of 2293 mAh·g<sup>-1</sup> was obtained for the hybrid Na-CO<sub>2</sub> battery using N-SWCNH as catalyst. Conversely, batteries with N-MWCNTs and AuNPs as catalysts displayed relatively lower discharge capacities of 2099 and 1701 mAh·g<sup>-1</sup>, respectively. The high specific capacity of Na-CO<sub>2</sub> battery with N-SWCNH as the catalyst is related to the large surface area of N-SWCNH, catalyst is related to the large surface area of N-SWCNH, allowing for the accumulation of discharge products, while porous conical structure ensure that the sufficient amounts of CO<sub>2</sub> and Na<sup>+</sup> are transferred to the electrode surface. Moreover, the stable discharge platform of 1.82 V for Na-CO<sub>2</sub> battery with N-SWCNH as the catalyst was observed during long time discharging, indicating that the N-SWCNH exhibited a high catalytic activity as a cathode in the hybrid Na-CO<sub>2</sub> battery.

The discharge curves of AuNPs, N-MWCNTs, and N-SWCNH were examined at various current densities, and the results are shown in Fig. 3e. With increasing the current density, a decrease of the discharge voltage and increase of the charge voltage for the three samples were obviously observed. During the discharge process, the discharge voltage of the N-SWCNH was higher than that of AuNPs at a current density of 0.1 mA cm<sup>-2</sup>. Furthermore, the discharge plateau of N-SWCNH was lower than that of AuNPs at other current densities, which could be the result of insufficient electronic conductivity of N-SWCNH [44]. However, the discharge voltage plateau of N-MWCNTs was lower than that of N-SWCNH at each current density owing to the low catalytic activity. During charging, the apparently low charge potential could be linked to decomposition of solid discharge products and the release of CO<sub>2</sub> evolution at catalytic cathode surface. The N-SWCNH with unique nanoporous structures offer more space for discharge products decomposition and substantial structural channels for CO<sub>2</sub> release. During the charge process, although charging voltage was similar, the charge voltage of the N-SWCNH was slightly lower than that of others at 0.5 mA cm<sup>-2</sup> to 1.5 mA cm<sup>-2</sup>, revealing the excellent electrochemical environment and catalytic activity of the N-SWCNH cathode. Although the electrocatalytic behavior of N-SWCNH is relatively worse than that of AuNPs during the discharge process, N-SWCNH is still an ideal catalyst for CO<sub>2</sub> electrocatalytic reduction reaction, because the battery with N-SWCNH as the catalyst exhibit high coulombic efficiency at low current densities, and the carbon source is extensive and inexpensive. This result confirmed that the N-SWCNH could be an ideal catalyst for the electrochemical reduction of CO<sub>2</sub> in the hybrid Na-CO<sub>2</sub> battery with saturated NaCl electrolyte. In addition, although our as-prepared hybrid Na-CO<sub>2</sub> battery exhibits extremely low overpotentials, compared with other CO<sub>2</sub> batteries [15,16], their rate capability still need to be improved because most of the electrode materials have poor diffusion kinetic properties of Na<sup>+</sup>, so it is difficult to achieve ideal capacity and rate performance. Therefore, the research and development of cathode materials is very important for the development and application of hybrid Na-CO<sub>2</sub> batteries.

Cycling stability is vital for practical applications. Hence, the stability of the hybrid Na-CO<sub>2</sub> battery was tested through continuous discharge-recharge cycling of at current density of 0.1 mA cm<sup>-2</sup>. As can be seen in Fig. 3f, the battery was able to be discharged and charged for over 300 cycles by refilling the catholyte, and displayed very stable charging-discharging voltages (in the inset of Fig. 3f). It is worth noting that the charging-discharging voltage gap increases significantly after about 305 cycles due to the poor density of deposited secondary Na as well as surface cracks in the pure Na anodes, which is unavoidable during long-term cycling [28,45]. This result indicates that hybrid Na-CO<sub>2</sub> battery exhibits an excellent cycle performance, which could be

not only credited to high catalysis activity of N-SWCNH but also the long-time chemically stable NASICON ceramics separator. The “dahlia-like” structure of N-SWCNH provides numerous reaction spaces to accumulate the discharge products, and assures sufficient diffusion of CO<sub>2</sub>, thus enhancing the reversibility. The NASICON effectively protects the anode compartment and avoids short-circuit contact between sodium dendrite and cathode, thereby ensuring long-term stable operation of the hybrid Na-CO<sub>2</sub> battery. Furthermore, in order to prevent the evaporation of the catholyte and maintain the long-term electrochemical performance of the hybrid Na-CO<sub>2</sub> battery, gel electrolyte or a circulation system of aqueous electrolyte with peristaltic pump can be utilized, the liquid anode could be a good selection to suppress sodium dendrites formation [25,28].

The resistances of the hybrid Na-CO<sub>2</sub> batteries at different conditions were investigated by electrochemical impedance spectroscopy (EIS) as manifested in Fig. S6. As shown in the inset of Fig. S6, an equivalent electric circuit was employed to simulate EIS. In the circuit, the high frequency intercept of semicircle on the real axis stands for the ohmic resistance (R<sub>e</sub>), which includes a bulk resistance of NASICON and the resistances of two liquid electrolytes. The small semicircle in the high frequency range reflect the interfacial resistances (R<sub>i</sub>), which is ascribed to the grain boundary resistance of NASICON and the interfaces resistance between the solid and liquid electrolytes. In the middle frequency region, the large semicircle corresponds to the resistance (R<sub>s</sub>) of a NASICON interphase on the sodium surface and the charge transfer resistance (R<sub>ct</sub>) in CO<sub>2</sub> electrode. CPE<sub>i</sub>, CPE<sub>s</sub>, and CPE<sub>ct</sub> reflect related capacitances described by the constant-phase elements. The lowest frequency range is characterized as finite length Warburg element (Z<sub>w</sub>), which arises from a diffusion process in the CO<sub>2</sub> electrode. These values of the equivalent circuit are summarized in Table S2. It is obvious that the total resistance of the battery at discharge stage after 20th cycling is larger than that of the charge stage after 20th cycling, corresponding to the increase in the three parts of resistances, namely, R<sub>e</sub>, R<sub>s</sub>, and R<sub>ct</sub>, resulting from the formation of solid electrolyte interphase on the sodium surface and the formation of discharge products with poor electrical conductivity on cathode. We also observe that the resistance of the 20th charged stage is slightly higher than that of the 1st charge stage, which is probably still some undecomposed discharge product after the 20th recharging, causing the increased interfaces resistance.

To verify the reaction mechanism, an in-situ Raman was designed to characterize the reaction products of discharge and charge. The assembled battery was put into a homemade device with a quartz window, thus the Raman signals from the cathode with N-SWCNH as catalyst can be captured through the quartz window. Before charging and discharging, the battery was placed in this device filled with highly pure CO<sub>2</sub> to stabilize for 30 min. The detailed structure of this device is shown in Fig. S7. One fixed point was selected to collect Raman spectra during the whole discharge and recharge process. As shown in Fig. 4a, Raman peaks of the N-SWCNH could be obviously obtained at 1350 cm<sup>-1</sup> (D band) and 1580 cm<sup>-1</sup> (G band). As the discharge continuing, a strong Raman peak at 1045 cm<sup>-1</sup> appeared and increased, this peak had been assigned to the symmetric stretching vibration of free CO<sub>3</sub><sup>2-</sup>, which corresponded to discharge product of Na<sub>2</sub>CO<sub>3</sub> [46]. The peak intensity of Na<sub>2</sub>CO<sub>3</sub> gradually increased and decreased during the discharging-charging process, suggesting the reversible generation and consumption of Na<sub>2</sub>CO<sub>3</sub>. The weak low frequency peak at 685 cm<sup>-1</sup> was also observed appearance and disappearance during discharge-charge due to the asymmetric bending mode of the CO<sub>3</sub><sup>2-</sup>, which also was considered as Na<sub>2</sub>CO<sub>3</sub> [46]. Moreover, in order to identify the discharge product of carbon, eliminating the signal of the carbon caused by N-SWCNH catalyst and other carbon species, a battery with AuNPs as catalyst without using carbon sources was also tested to confirm the existence of carbon in the discharge products. As shown in Fig. S8, at the beginning of the discharge, the Raman peak corresponding to Na<sub>2</sub>CO<sub>3</sub>. The intensity of D and G bands of carbon increased with increasing the discharge time, illustrating the existence of Na<sub>2</sub>CO<sub>3</sub> and carbon in the

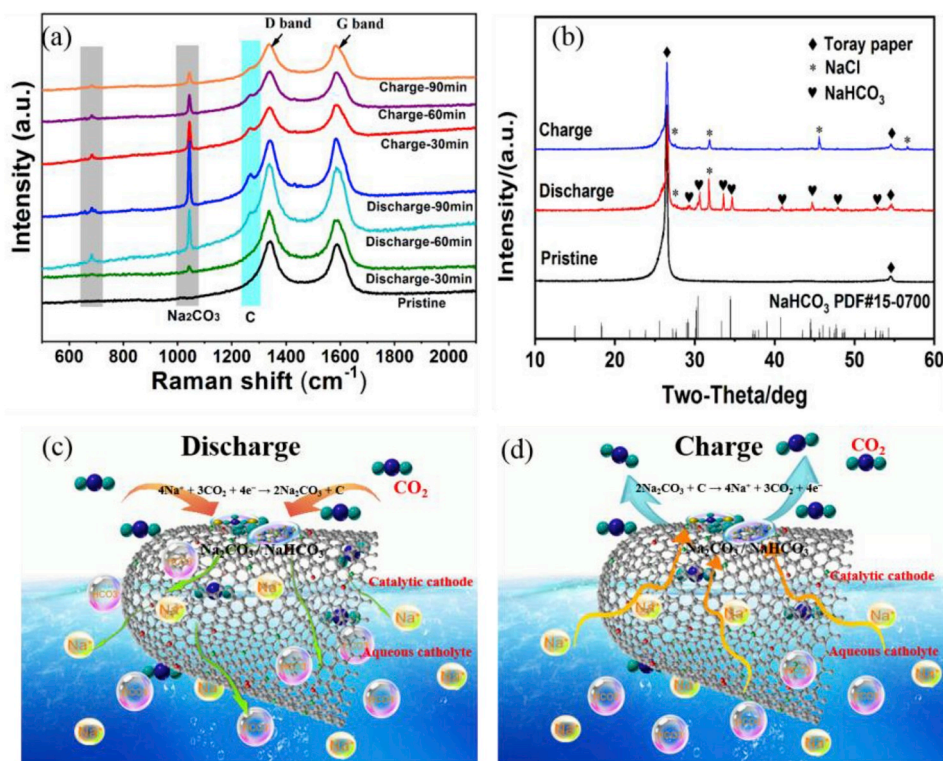


**Fig. 4.** (a) In-situ Raman characterization of the hybrid Na-CO<sub>2</sub> battery during discharge and recharge, (b) Ex-suit XRD pattern of the CO<sub>2</sub> electrode after discharge and charge. (c, d) Schematic diagrams of the discharge and charge reactions occurring in the hybrid Na-CO<sub>2</sub> battery with N-SWCNH as a catalyst and the NaCl solution as an aqueous catholyte, respectively.

discharge products. Furthermore, the high frequency Raman bands at  $1268\text{ cm}^{-1}$  observed in Fig. 4a may be attributed to the C-C bond skeletal stretching modes, indicating that there may be a new type of carbon, this is likely to form a carbon nanohoops caused by N-SWCNH [47]. The peak intensity of new C appears and increases with discharging, then decreases and disappears with increasing charging time. Furthermore, we investigated the deposition of Na in hybrid Na-CO<sub>2</sub> batteries replacing sodium by nickel foam as substrate, NaCl solution as catholyte and Na<sub>2</sub>CO<sub>3</sub>/N-SWCNH as the cathode (Fig. S9-10). As shown in Fig. S9 (a), the result of XRD proves that metal sodium has been deposited on foam nickel after charging. The ex-suit XRD was also implemented to verify the discharged product in Fig. 4b. Astonishingly, the results of ex-suit XRD showed that the discharged product was NaHCO<sub>3</sub>, which were different from in-suit Raman results. However, it is easily understandable and acceptable that the generated Na<sub>2</sub>CO<sub>3</sub> combined with H<sub>2</sub>O and CO<sub>2</sub> to form NaHCO<sub>3</sub> in aqueous electrolyte during a long time discharge process. Since Raman spectroscopy has a low sensitivity for HCO<sub>3</sub><sup>-</sup>, it is difficult to determine the presence of a small amount of HCO<sub>3</sub><sup>-</sup>. After charging process, almost no peak of NaHCO<sub>3</sub> is detected, suggesting the hybrid Na-CO<sub>2</sub> battery is completely reversible. The SEM image of N-SWCNH electrode after completely discharging and the corresponding elemental mapping of C, O and Na are shown in Fig. S11. It can be seen that the N-SWCNH electrode is covered by discharge products, which are agglomerated to form villous or urchin-like. In addition, the energy dispersive X-ray analyzer (EDX) is also implemented to characterize the discharge product (Fig. S12). Combined with the results of in situ Raman and ex-suit XRD, we could discuss the possible generation mechanism of the hybrid Na-CO<sub>2</sub> battery on N-SWCNH catalytic cathode, as schematically illustrated in Fig. 4c and d. During discharge process the CO<sub>2</sub> adsorbed on the N-SWCNH combines with the transferred sodium ions and electrons to form Na<sub>2</sub>CO<sub>3</sub> and carbon on the surface of N-SWCNH, and then partial Na<sub>2</sub>CO<sub>3</sub> turns into NaHCO<sub>3</sub>. While during charge process, Na<sub>2</sub>CO<sub>3</sub> and carbon will be decomposed back into Na<sup>+</sup> and CO<sub>2</sub>. We also observed that a small amount of Na<sub>2</sub>CO<sub>3</sub>

existed upon charging (Fig. 4a). We believe that not fully decomposed discharge product are accumulated during long-period cycling, which is associated with the increase of charging voltage and polarization. However, it is not clear the existence form of the discharge product C at present, therefore, some detailed studies on the influence of reaction process towards the existence form and morphology of the discharge product C in Na-CO<sub>2</sub> battery with N-SWCNH as the catalyst are still required.

#### 4. Conclusion

In summary, a novel rechargeable hybrid Na-CO<sub>2</sub> battery using a NASICON solid electrolyte to separate aqueous electrolyte and nonaqueous electrolyte and N-SWCNH as a catalyst was fabricated successfully, and demonstrated satisfactory electrochemical performances. The as-prepared hybrid Na-CO<sub>2</sub> battery not only exhibited a low discharge/charge voltage gap of 0.49 V at a current density of  $0.1\text{ mA cm}^{-2}$ , which corresponds to a high round trip efficiency of 81.3% for the first cycle, but also offered a high discharge capacity of  $2293\text{ mAh g}^{-1}$  with a cut-off voltage of 1.0V at current density of  $0.2\text{ mA cm}^{-2}$ , and was able to cycle over 300 times at current densities of  $0.1\text{ mA cm}^{-2}$  and no significant degradation was observed. Na<sub>2</sub>CO<sub>3</sub> and carbon were also confirmed to be the main discharge products by in situ Raman spectra. The NASICON is effective to eliminate short circuit during cycling, which improves the safety and enables the long-term charge-discharge of hybrid Na-CO<sub>2</sub> battery. A large number of potential defect sites in unique conical porous structure, and N dopants make N-SWCNH itself have good wettability and electronic affinity, as well as CO<sub>2</sub> adsorption/desorption ability, which demonstrates excellent and durable electrocatalytic activity as the catalyst for hybrid Na-CO<sub>2</sub> battery. These results provide an incentive and promising approach for reliable, cost efficient, and green utilization and capture of CO<sub>2</sub>, enabling the achievement of next-generation energy storage and release systems.

## Declaration of competing interest

The authors declare that they have no known competing financial interests or personal relationships that could have appeared to influence the work reported in this paper.

## Acknowledgement

This work was financially supported by the National Natural Science Foundation of China (51704136, 11765010), the Applied Basic Research Programs of Yunnan Provincial Science and Technology Department (2016FB087), the project of Academician free exploration project of Yunnan Province (2018HA006), the Program for Innovative Research Team in University of Ministry of Education of China (IRT17R48). This research was supported by Natural Sciences and Engineering Research Council of Canada, Canada Research Chair Program, and the University of Western Ontario.

## Appendix A. Supplementary data

Supplementary data to this article can be found online at <https://doi.org/10.1016/j.nanoen.2019.104318>.

## References

- [1] J.D. Shakun, P.U. Clark, F. He, S.A. Marcott, A.C. Mix, Z. Liu, B. Ottobliesner, A. Schmittner, E. Bard, *Nature* 484 (2012) 49–54.
- [2] Z. Xie, X. Zhang, Z. Zhang, Z. Zhou, *Adv. Mater.* 29 (2017) 1605891.
- [3] W. Yang, K. Dastafkan, J. Chen, C. Zhao, *Adv. Mater. Technol.* 3 (2018) 1700377.
- [4] Z. Fei, B. Jiwoong, Z. Xingyi, G. Youhong, Y. Guihua, *Adv. Mater.* 30 (2018) 1801796.
- [5] S. Xu, S.K. Das, L.A. Archer, *RSC Adv.* 3 (2013) 6656–6660.
- [6] W. Ma, X. Liu, C. Li, H. Yin, W. Xi, R. Liu, G. He, X. Zhao, J. Luo, Y. Ding, *Adv. Mater.* 30 (2018), e1801152.
- [7] Y. Liu, W. Rui, Y. Lyu, L. Hong, L. Chen, *Energy Environ. Sci.* 7 (2014) 677–681.
- [8] X. Hu, J. Sun, Z. Li, Q. Zhao, C. Chen, J. Chen, *Angew. Chem.* 128 (2016) 6592–6596.
- [9] X. Li, S. Yang, N. Feng, P. He, H. Zhou, *Chin. J. Catal.* 37 (2016) 1016–1024.
- [10] S. Xu, Y. Lu, H. Wang, H. Abruna, L. Archer, *J. Mater. Chem. A.* 2 (2014) 17723–17729.
- [11] S. Xu, S. Wei, H. Wang, H.D. Abruna, L.A. Archer, *ChemSusChem* 9 (2016) 1600–1606.
- [12] Z. Xin, Z. Qiang, Z. Zhang, C. Yanan, X. Zhaojun, W. Jinping, Z. Zhen, *Chem. Commun.* 51 (2015) 14636.
- [13] Y. Wang, C. Li, Z. Guo, B. Yang, Y. Liu, Y. Xia, *Angew. Chem.* 129 (2017) 9126–9130.
- [14] X. Hu, Z. Li, Y. Zhao, J. Sun, Q. Zhao, J. Wang, Z. Tao, J. Chen, *Sci. Adv.* 3 (2017), e1602396.
- [15] Z. Zhang, Z. Qiang, C. Yanan, B. Jie, Z. Xianlong, X. Zhaojun, W. Jinping, Z. Zhen, *Angew. Chem.* 54 (2015) 6550–6553.
- [16] L. Qie, Y. Lin, J.W. Connell, J. Xu, L. Dai, *Angew. Chem. Int. Ed.* 129 (2017) 6970.
- [17] S. Yang, Y. Qiao, P. He, Y. Liu, Z. Cheng, J.-j. Zhu, H. Zhou, *Energy Environ. Sci.* 10 (2017) 972–978.
- [18] S. Li, D. Yu, J. Zhou, L. Yuan, J. Wang, G. Xing, Y. Han, P. Qi, W. Bo, *Energy Environ. Sci.* 11 (2018), 10.1039.C1038EE00415C.
- [19] Y. Hou, J. Wang, L. Liu, Y. Liu, S. Chou, D. Shi, H. Liu, Y. Wu, W. Zhang, J. Chen, *Adv. Funct. Mater.* 27 (2017) 1700564.
- [20] C. Fang, J. Luo, C. Jin, H. Yuan, O. Sheng, H. Huang, Y. Gan, Y. Xia, C. Liang, J. Zhang, *ACS Appl Mater Inter* 10 (2018) 17240–17248.
- [21] X. Wang, J. Xie, M.A. Ghausi, J. Lv, Y. Huang, M. Wu, Y. Wang, J. Yao, *Adv. Mater.* (2019) 1807807.
- [22] T. Liu, B. Wang, X. Gu, L. Wang, M. Ling, G. Liu, D. Wang, S. Zhang, *Nano Energy* 30 (2016) 756–761.
- [23] H. Wang, T. Zhang, C. Chen, M. Ling, Z. Lin, S. Zhang, F. Pan, C. Liang, *Nano Res* 11 (2018) 490–498.
- [24] Y. Kim, H. Kim, S. Park, I. Seo, Y. Kim, *Electrochim. Acta* 191 (2016) 1–7.
- [25] S. Senthilkumar, J. Han, J. Park, S.M. Hwang, D. Jeon, Y. Kim, *Energy Storage Mater.* 12 (2018) 324–330.
- [26] T. Hashimoto, K. Hayashi, *Electrochim. Acta* 182 (2015) 809–814.
- [27] F. Liang, K. Hayashi, *J. Electrochem. Soc.* 162 (2015) A1215–A1219.
- [28] L. Feng, X. Qiu, Q. Zhang, K. Yao, A. Koo, K. Hayashi, K. Chen, D. Xue, K.N. Hui, H. Yadegari, *Nano Energy* 49 (2018). S2211285518303045.
- [29] K. Hayashi, K. Shima, F. Sugiyama, *J. Electrochem. Soc.* 160 (2013) A1467–A1472.
- [30] H. Park, K. Jung, M. Nezafati, C.S. Kim, B. Kang, *ACS Appl Mater Inter* 8 (2016) 27814–27824.
- [31] D. Zhang, K. Ye, Y.C. Yao, F. Liang, T. Qu, W.H. Ma, B. Yang, Y.N. Dai, T. Watanabe, *Carbon* 142 (2019) 278–284.
- [32] Z.A. Xiong, S. Liao, D. Dai, X. Tian, S. Hou, F. Liu, H. Peng, Z. Fu, *Int. J. Hydrogen Energy* 40 (2015) 3961–3967.
- [33] Y. Kang, D. Zou, J.Y. Zhang, F. Liang, K. Hayashi, H. Wang, D.F. Xue, K.F. Chen, K. R. Adair, X.L. Sun, *Electrochim. Acta* 244 (2017) 222–229.
- [34] Y.Q. Wu, X.C. Qiu, F. Liang, Q.K. Zhang, A. Koo, Y.N. Dai, Y. Lei, X.L. Sun, *Appl. Catal. B Environ.* 241 (2019) 407–414.
- [35] S. Iijima, M. Yudasaka, R. Yamada, S. Bandow, K. Suenaga, F. Kokai, K. Takahashi, *Chem. Phys. Lett.* 309 (1999) 165–170.
- [36] N. Karousis, I. Suarezmartinez, C.P. Ewels, N. Tagmatarchis, *Chem. Rev.* 116 (2018) 4850.
- [37] J.R. Pels, F. Kapteijn, J.A. Moulijn, Q. Zhu, K.M. Thomas, *Carbon* 33 (1995) 1641–1653.
- [38] X.Q. Lin, W.D. Wang, Q.F. Lü, Y.Q. Jin, Q. Lin, R. Liu, J. Mater. Sci. Technol. 33 (2017). S1005030217301573.
- [39] R.T. Lv, T.X. Cui, M.S. Jun, Q. Zhang, A.Y. Cao, D.S. Su, Z.J. Zhang, S.H. Yoon, J. Miyawaki, I. Mochida, F.Y. Kang, *Adv. Funct. Mater.* 21 (2011) 999–1006.
- [40] Y. Chen, C.W. Li, M.W. Kanan, *J. Am. Chem. Soc.* 134 (2012) 19969–19972.
- [41] C. Rogers, W.S. Perkins, G. Veber, T.E. Williams, R.R. Cloke, F.R. Fischer, *J. Am. Chem. Soc.* 139 (2017) 4052–4061.
- [42] J.J. Wu, R.M. Yadav, M.J. Liu, P.P. Sharma, C.S. Tiwary, L.L. Ma, X.L. Zou, X. D. Zhou, B.I. Yakobson, J. Lou, P.M. Ajayan, *ACS Nano* 9 (2015) 5364–5371.
- [43] U. Gulzar, T. Li, X. Bai, M. Colombo, A. Ansaldo, S. Marras, M. Prato, S. Goriparti, C. Capiglia, R. Proietti Zaccaria, *ACS Appl Mater Inter* 10 (2018) 5551–5559.
- [44] Y. Zhao, J. Li, Y. Ding, L. Guan, *RSC Adv.* 1 (2011) 852–856.
- [45] K. Yao, F. Su, Q. Zhang, L. Feng, K.R. Adair, K. Chen, D. Xue, K. Hayashi, C.C. Shan, H. Yadegari, *ACS Appl Mater Inter* 10 (2018) 23748–23756.
- [46] N. Buzgar, A.I. Apopei, *Geologie Tomul* 2 (2009) 97–112.
- [47] H. Chen, M.R. Golder, F. Wang, R. Jasti, A.K. Swan, *Carbon* 67 (2014) 203–213.